Journal of Molecular Liquids 223 (2016) 652–659

Contents lists available at ScienceDirect

Journal of Molecular Liquids

journal homepage: www.elsevier.com/locate/molliq

Intermediate state created by dopant ions (Mn, Co and Zr) into TiO_2 nanoparticles for degradation of dyes under visible light

Lalitha Gnanasekaran [a,*], R. Hemamalini [a,*], Rajendran Saravanan [b], K. Ravichandran [c], F. Gracia [b], Vinod Kumar Gupta [d]

[a] Department of Physics, Queen Mary's College, Chennai 600 004, India
[b] Department of Chemical Engineering and Biotechnology, University of Chile, Beauchef 850, Santiago, Chile
[c] Department of Nuclear Physics, University of Madras, Guindy Campus, Chennai 600 025, India
[d] Department of Applied Chemistry, University of Johannesburg, Johannesburg, South Africa

ARTICLE INFO

Article history:
Received 11 July 2016
Received in revised form 24 August 2016
Accepted 29 August 2016
Available online 30 August 2016

Keywords:
Photocatalyst
Intermediate states
Surface area
Visible light
Doped materials

ABSTRACT

To expand the absorption of pure nanosized TiO_2 to the visible light range for improving the photocatalytic efficiency necessary for industrial application, the way of doping different transition metals such as Mn, Co and Zr into TiO_2 was done by sol-gel synthesis method. The X-ray diffraction studies were identified that the metal doped TiO_2 and undoped TiO_2 samples have the same tetragonal structure with pure anatase phase. Obviously, the crystallite size is smaller for the doped materials than that of pure TiO_2 sample. The characteristic FE-SEM images revealed well distributed spherical shaped particles. The dopant materials induced significant changes in the surface area of TiO_2 which was confirmed by Brunauer Emmet Teller method. The absorption edge of doped TiO_2 is at a higher wavelength that corresponds to red region, because of the formation of intermediate states in the doped metal ions into TiO_2 sites. Moreover, for the photocatalytic degradation of MB and MO dyes, the prepared catalysts were tested under both UV and visible light irradiation. The observation confirms that among all the other samples, Mn doped TiO_2 shows amazing photocatalytic performance in visible light due to its smaller crystallite size, large surface area and lower band gap.

1. Introduction

Water pollutants may exist in different hazardous wastes like pharmaceutical wastes, pesticides, herbicides, textile dyes, resins and phenolic compounds [1–2]. In the modern era, water pollution has become the finest topic to discuss because of depleting underground water resources and the lack of managing waste water, which ensures unsustainable life with safe water. Even, very lesser amounts of water effluents promote adverse health effects in humans and other ecosystems. Hence, industrial discharge of waste water needs proper sewage treatment plants for the essential waste water management [1–4]. Waste water treatment technologies have come across with various efficient methods, but cheaper and less time consuming method is a major tool to access safe water [5]. The powerful method of waste water recycling has been done with the cost effective advanced oxidation processes (AOPs). Waste water treatment of water splitting on TiO_2 electrode by means of heterogeneous photocatalysis under UV light irradiation was experimented by Fujishima and Honda in 1972 [6]. Thus, photocatalysis is intended for modern day researchers to accomplish the complete degradation of waste water by decaying the harmful chemical effluents present in waste water [3,4]. Oxidation of waste water also requires another influential method in AOP called the Photo-Fenton process. Photocatalytic process benefits over this method by the unessential requirement of any chemicals other than the catalyst. In general, photocatalysis means "speeding up of a chemical reaction by an appropriate light source" [3–4,6].

In recent years, addressing and resolving of various environmental issues is a globally needed task and so the researchers make use of metal oxide semiconductor nanomaterials [7]. Inspite of many researchers conducted to study about the activity of semiconductor photocatalysts, titanium dioxide (TiO_2) is one of the noticeable photocatalysts which has peculiar properties to function as a recoverable and reusable catalyst, which offers an eco-friendly and non-toxic approach. Also, it has favorable bandgap energy, high chemical stability, photostability, corrosive resistant, high refractive index, high dielectric constant and low cost availability [8–9]. The production of more electrons and holes is an essential step in the photocatalytic degradation of harmful species in waste water [8–9]. TiO_2 has three phases including anatase, rutile and brookite of which the most sensitive and attractive phase is the anatase phase having a notable photocatalytic activity due to its thermal stability and adsorption power [10–11].

* Corresponding authors.
E-mail addresses: lalitha1887@gmail.com (L. Gnanasekaran), hemaphy.qmc@gmail.com (R. Hemamalini).

http://dx.doi.org/10.1016/j.molliq.2016.08.105
0167-7322/

Poor efficiency of visible light response tends to the limitation of using pure TiO_2, due to its large band gap which hinders the catalysts inefficiency to degrade under natural sunlight illumination, as the solar spectrum contains more visible region [12–14]. Doping of TiO_2 with different metals (Ce, Co, Cu, Fe, Mn, Mo, Ni, Y, V, Cr and Zr) possess more degradation efficiency under visible light, which attains the successful waste water treatment process [13–15]. Moreover, the particle size is reduced by the incorporation of dopant material into the semiconductor material to facilitate an essential role in obtaining better activity of the photocatalyst [13–15]. Further, catalysts modification improves the band gap reduction and this is achieved by doping with different synthesis process. [15–16]. Choina et al. reported that higher pollutant concentration with increase of zirconium (Zr) doping TiO_2 catalyst at the surface has shown higher activity and excellent adsorption properties in low concentrated aqueous solution due to larger surface area [17]. On the other hand, Cobalt (Co) doped TiO_2 is an efficient and stable photocatalyst for continuous hydrogen production from glycerol aqueous solution under solar light irradiation due to band gap alteration which induces the synergistic effects [18]. The work of Deng et al. [19] had showed that Mn doping with TiO_2 induced the narrow band gap under visible light degradation of methylene blue dye. While increasing Mn content, it greatly increases the absorption in the red region of the spectrum and promotes narrowing of band gap by providing better degradation of the photocatalysts [19]. Another literature had reported the synthesis of co-doping TiO_2 with Fe and N by sonochemical method and the results exhibited the anatase phase crystalline structure in which the TiO_2 absorption edge has been red shifted so that the catalyst has exhibited good photocatalytic performance due to the hindering of electron-hole pairs recombination on the degradation of dye under natural sunlight [20]. Besides, the doping of TiO_2 with transition metals like Mn, Ni, Fe were employed in various other applications [21–23].

The major curiosity of the present task is implied on the preparation of anatase phase nanosized pure TiO_2 semiconductor and doping with various transition metals include manganese (Mn), cobalt (Co) and zirconium (Zr) by sol-gel process. Later, the calcination of the catalysts was followed at 450 °C uniform temperature for 1 h. Further, the prepared catalysts were performed with various analytical techniques and the detailed results are obtained. The dopant materials have induced enhanced photocatalytic performance under UV and visible light condition. The visible light photocatalytic mechanism and their corresponding experimental observations are explained in detail.

2. Experimental procedure

2.1. Materials

Titanium tetra isopropoxide (TTIP), isopropyl alcohol, cetyl trimethyl ammonium bromide (CTAB), subsequent doped metal sources (manganese nitrate, cobalt nitrate and zirconium propoxide) and for photocatalytic degradation, the methylene blue (MB) and methyl orange (MO) dyes were obtained from Sigma Aldrich. Double distilled water is used for preparing all aqueous solutions.

2.2. Synthesis of pure TiO_2

At first, the pure TiO_2 nanomaterial has been prepared by sol-gel method and their consequent steps are clearly represented in a flowchart (Fig. 1).

Initially, isopropyl alcohol of 150 mL was taken in a 500 mL beaker. Then, 5 mL TTIP was taken in a syringe and instantly transferred to the above solution contained in the beaker, since TTIP has the ability to change its state rapidly. Magnetic stirring of this solution was done for more than 1 h and by this time, aqueous CTAB of 0.01 M was slowly added in drops into it. Stirring of the solution has been continued for another 24 h. Now, this solution mixture was transformed to a dirty white gel in the beaker, where it was left for drying at room temperature.

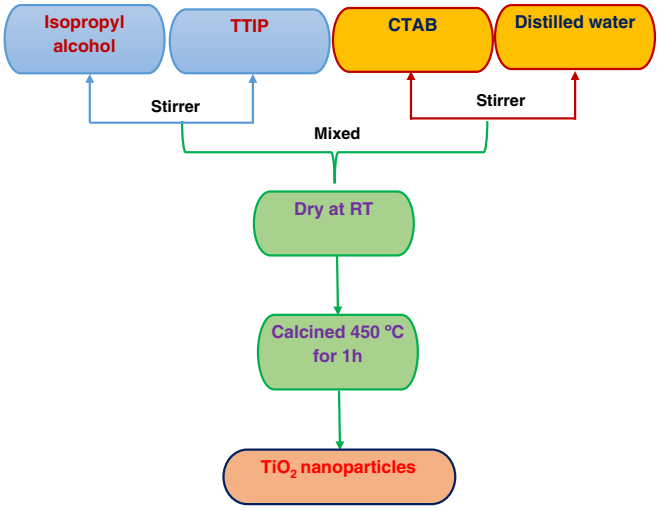

Fig. 1. Flow chart represented pure TiO_2 nanoparticles preparation.

Later, the powder was grounded taking in the mortar and was allowed placing in a muffle furnace for calcining at 450 °C for 1 h in which the rate of 4 °C temperature per minute has been increased.

2.3. Synthesis of Mn, Co and Zr doped TiO_2 nanomaterials

The main goal of this paper is to report on the dopant materials induced photocatalytic activity by the use of the prepared catalysts synthesized by a simple sol-gel method. While preparing pure TiO_2, 95:5 weight ratios of TTIP and the metal sources of each element (Manganese nitrate, Cobalt nitrate and Zirconium propoxide) were mixed independently and the above same procedure was followed.

2.4. Photocatalytic experiment

The scrutinization of photocatalytic activity of the catalysts is performed for the degradation of dye solutions at uniformly irradiated time intervals. The samples were then collected, centrifuged, filtered and analyzed by UV–Visible spectrophotometer. Without the presence of catalysts, the dyes were first tested for its stability. Under UV light irradiation, magnetic stirring of the aqueous dye solutions of MB and MO were carried out under dark condition for 2 h. While analyzing through UV–Vis spectrophotometer, no change was observed in the solution concentration and this ensures the stability. To avoid the direct contact of light source with the dye solution, a cylindrical glass tube made of quartz is used to cover the UV light source of 8 W mercury vapor lamp having a wavelength of 365 nm. The photocatalytic mixture is well prepared in a 500 mL cylindrical beaker by taking 100 mg of prepared catalyst in 100 ml of dye solution (MB/MO) with an initial concentration of 5×10^{-5} mol/L. To maintain a constant temperature of the solution at 25 °C, the beaker is surrounded by a water jacket and this was stirred 20 min magnetically under the dark condition to ensure adsorption/desorption equilibrium condition. For every 20 min, the sample was collected, centrifuged and filtered. Then the samples were analyzed by UV–Vis spectrophotometer and the degradation efficiencies of MO and MB were determined by the following formula.

$$\eta = [1 - C/C_0] \times 100 \quad (1)$$

where, C_0 and C are the concentrations of the solution before illumination ($t = 0$) and after illumination of light for 't' minutes respectively. For visible light degradation of dyes, experiment involves a photo reactor set up which has a visible light source (SCIENCETECH, model no: SF300B along with AM 1.5G filter which is due to given standard solar

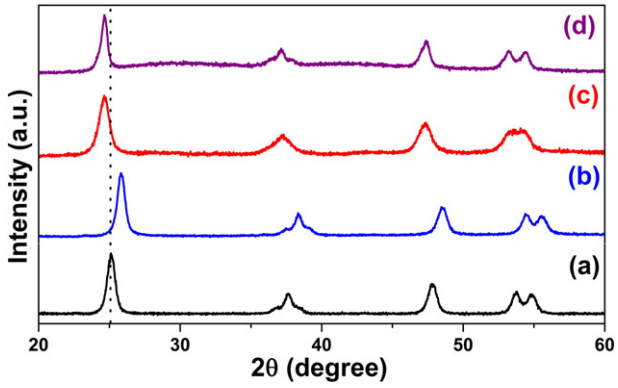

Fig. 2. The XRD pattern of a) pure TiO_2, b) Mn doped TiO_2, c) Co doped TiO_2 and d) Zr doped TiO_2.

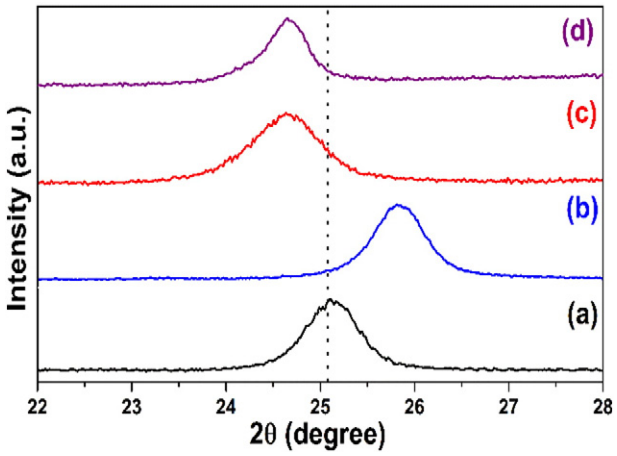

Fig. 3. The higher intensity (101) XRD peak of a) pure TiO_2, b) Mn doped TiO_2, c) Co doped TiO_2 and d) Zr doped TiO_2.

spectrum). For photocatalytic reaction mixtures, the dye solutions were prepared same as for the above procedure.

2.5. Characterization results

The analysis of structure, phase and crystallite size of the prepared samples were obtained from X-ray diffraction method using a D5000 (Siemens) diffractometer with $CuK_{\alpha 1}$ ($\lambda = 1.5406$ Å) radiation. The studies on the surface morphology of the prepared samples were analyzed with FEI quanta FEG 200-Field emission Scanning Electron Microscope. Energy dispersive X ray spectroscopy (EDXS) analysis was done for finding out the existence of elements in the samples. The specific surface area was calculated using Brunauer–Emmett–Teller (BET, Micromeritics ASAP 2020, USA) equation. The prepared catalysts were examined through UV–visible spectrophotometer (RX1, Perkin – Elmer, USA) to obtain the exact bandgap and also their photocatalytic activities were evaluated.

3. Results and discussion

The X-ray diffraction patterns of 450 °C calcined pure and metal doped TiO_2 were presented in Fig. 2. The XRD pattern of pure TiO_2 depicted in Fig. 2(a) shows well identified tetragonal structure anatase phase with no other phase entries like rutile and brookite. On comparing with other phases, anatase phase is proven best due to its large band gap of 3.2 eV, which has an ability to undergo lesser adsorption of light energy by improving electron excitation from lower to the higher energy state. Hence the molecules of adsorbed TiO_2 promote more oxidation and make available transfer of electrons from TiO_2 surface [10–11].

Even doping Mn, Co and Zr with TiO_2 resulted in the restriction of the structural and phase transformation, hence remains the same anatase phase tetragonal structure which is shown in Fig. 2(b), (c) and (d). The diffracted crystalline peaks at the corresponding 2θ values 25.3°, 37.01°, 37.8°, 38.64°, 48.14°, 53.97°, 55.18° were assigned to the (101), (103), (004), (112), (200), (105) and (211) hkl planes respectively, which was well matched with the JCPDS card no 89-4921. The crystallite size is obtained from the full width half maximum of the higher intensity (101) peak using Scherrer formula [15].

$$D = K\lambda/\beta\cos\theta \quad (2)$$

where D is the crystallite size of the material, K is the shape factor = 0.9, λ is the wavelength of the x-ray (0.154 nm), β is the line broadening at half the maximum intensity of the diffracted peaks, θ is the Bragg's angle and the calculated crystallite size values of the samples are listed in Table 1.

The higher intensity (101) peak of the synthesized samples was shown in Fig. 3. In Fig. 3(b), Mn doped TiO_2 peaks exhibit higher angle shift. Besides, adding Co and Zr impurities to TiO_2 shown in Fig. 3(c) and (d) indicate the lower angle shift when compared with pure TiO_2 (Fig. 3 (a)). These results confirm the shifting of diffraction peaks consisting of doped metals in which the Mn^{4+} (0.55 Å), Co^{2+} (0.65 Å) and Zr^{4+} (0.72 Å) ions are substituted into the Ti^{4+} (0.61 Å) sites. When compared with pure Ti^{4+} site, the ionic radius which seems to be lower in Mn^{4+} stimulates the peaks to shift into higher angle [24]. But, Co^{2+} and Zr^{4+} having higher ionic radius induce lower shift compared to the TiO_2 which has low ionic radius [16,25]. On observing the doped sites, there was a slight decrease in the peak intensity and the peaks are wider. Thus, it results increase in full width half maximum and induces the doped TiO_2 to exhibit smaller crystallite size, while larger crystallite size is observed in pure TiO_2 which is in agreement with the previous reports [24–27].

Hence, from the XRD results, it is evident that none of the dopant elements disturb the anatase structure of TiO_2. So it clearly represents that the dopant materials were not observable on the TiO_2 surface, because of the absence of any secondary structure; instead it may exists at the grain boundaries that hinder the crystallinity and reduce the crystallite size of the doped TiO_2 materials [24–27].

The size and morphology of the prepared samples and the distribution of the dopant metals on the TiO_2 catalyst were characterized using FE-SEM technique. The FE-SEM image of pure TiO_2 presented in Fig. 4(a) shows a closer study of more spherical shaped particles which has agglomeration of densely packed nanoparticles. Fig. 4(b), (c) and (d)

Table 1
Crystallite size, surface area, absorption wavelength and bandgap values of all prepared samples.

Samples	Crystallite size-D (nm)	BET surface area (m^2/g)	Absorption wavelength (nm)	Bandgap-E (eV)
Pure TiO_2	19.3	73.8	382	3.25
Mn doped TiO_2	13.2	86.5	423	2.93
Co doped TiO_2	14.5	79.3	411	3.01
Zr doped TiO_2	18.3	74.2	401	3.09

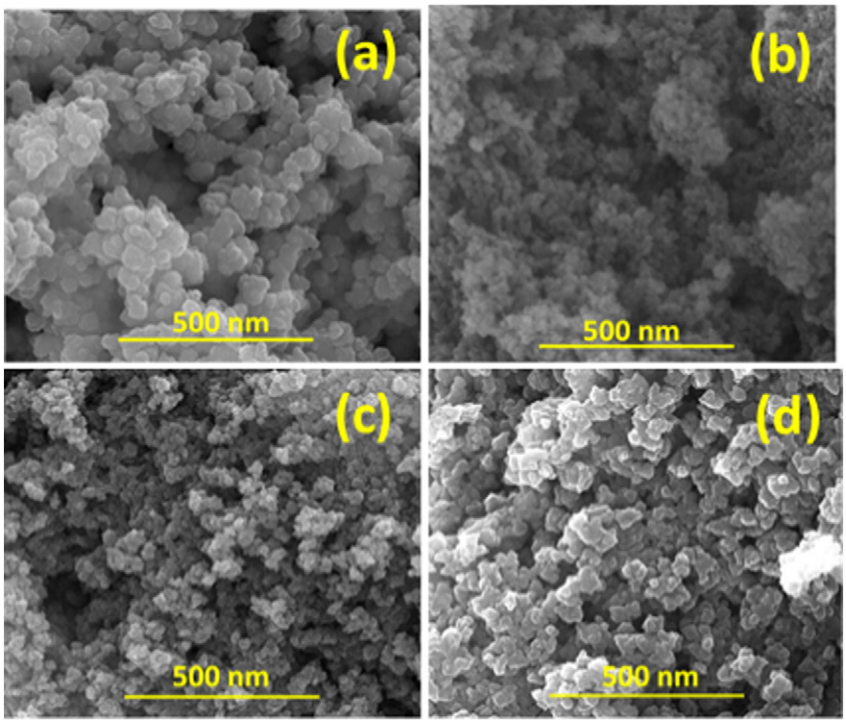

Fig. 4. FE-SEM images of a) pure TiO_2, b) Mn doped TiO_2, c) Co doped TiO_2 and d) Zr doped TiO_2.

apparently show the spherical shaped Mn, Co and Zr doped TiO_2 nanostructures. On comparing pure TiO_2 images with the doped ones, the later show ultra-fine nanoparticles. The obtained average size of the TiO_2 nanoparticles is about 30–35 nm, whereas the doped TiO_2 is in

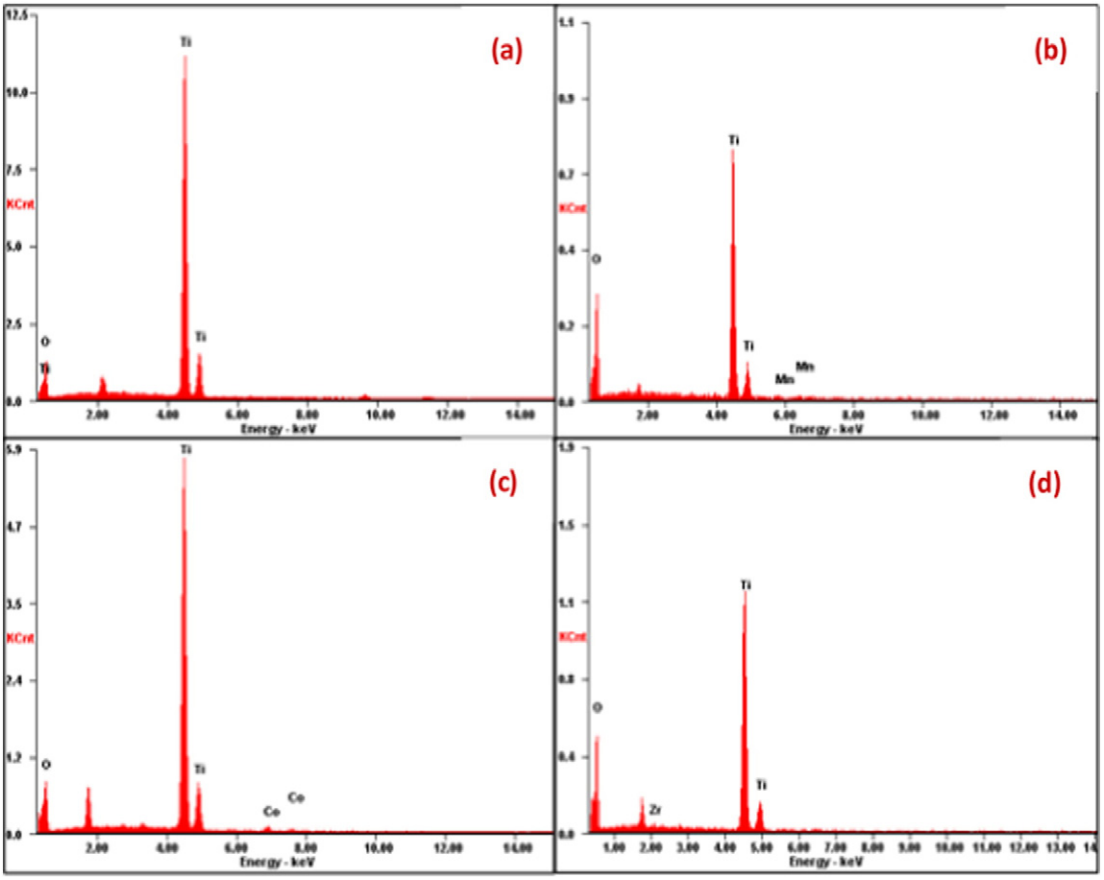

Fig. 5. EDS of a) pure TiO_2, b) Mn doped TiO_2, c) Co doped TiO_2 and d) Zr doped TiO_2.

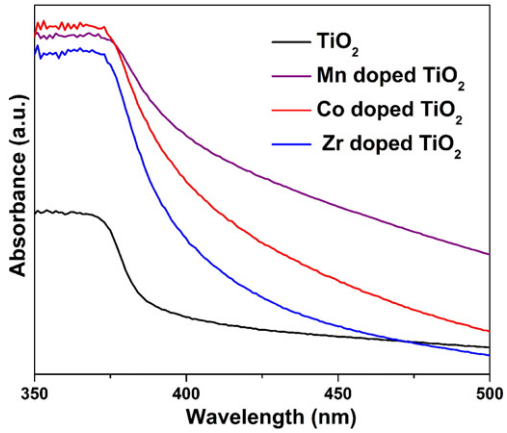

Fig. 6. UV–Visible absorption spectrum of all prepared samples.

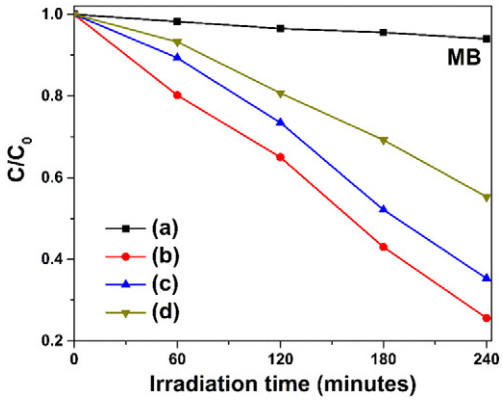

Fig. 7. Time course degradation of MB under visible light using a) pure TiO_2, b) Mn doped TiO_2, c) Co doped TiO_2 and d) Zr doped TiO_2.

range of 18–25 nm. The attractive morphology of the samples was useful for the study of structural properties and also for modifying the electronic structure in order to obtain higher photocatalytic activity under visible light [28].

The energy dispersive x-ray spectra (EDXS) of pure and doped TiO_2 were shown in Fig. 5, which indicates the elements present in the sample. Fig. 5(a) represents the occurrence of Ti and O elements in the pure TiO_2 nanoparticle. The other doped nanoparticles in the Fig. 5(b), (c) and (d) exhibit the existence of Ti, O, Mn, Co and Zr elements in the samples. The occurrence of Ti arises as large intensity peaks; whereas the lower intensity peaks were recognized as Co, Mn and Zr. From this observation, it is evident that the dopant metals are evenly scattered on the TiO_2 surface.

The Bruner Emmet Teller (BET) specific surface area of pure and doped samples is listed in Table 1. The surface area of the metal doped TiO_2 is well observed higher than that of pure TiO_2, because of the synergetic effect between TiO_2 and doped metal ions [29–32]. This in fact reduces the crystallite size of the doped materials. Large surface area induces photocatalytic enhancement and so the photocatalytic efficiency is more profitable by the advancement of redox reaction to occur with the modified surface property of the doped TiO_2 [29–32]. Moreover, these results had good agreement with XRD and FE-SEM results.

The electronic structure of the samples to function as the optical properties such as absorption and band gap by the irradiating light intensity was determined from UV–Visible spectroscopic analysis.

Fig. 6 illustrates the UV–Visible absorption spectra of pure and doped samples. From the absorption spectrum, it is noticeable that the optical absorption edge of the pure samples is at a wavelength of 382 nm. In contrast, impurities added TiO_2 signify higher wavelength which corresponds to red region of the solar spectrum. The band gap of the samples can be obtained using the following equation.

$$E = h\nu = 1240/\lambda \quad (3)$$

where h is the planck's constant, ν is the frequency of light waves and λ is the wavelength of the light used.

The pure TiO_2 belongs to higher band gap (3.25 eV) and this band gap energy is sufficient to produce electrons and holes during the UV light irradiation. Simultaneously, pure TiO_2 is impotent to degrade dyes under visible light. In contrast, after doping of metal ions into TiO_2, the absorption edge shows higher wavelength due to the formation of intermediate states produced by metal ions into the TiO_2 structure [33–34]. Consequently, the UV absorption of the dopant material is favorable to achieve higher degradation efficiencies under both UV and visible light irradiation.

3.1. Photocatalytic degradation of MB and MO

The photocatalytic reaction event does not happen without the catalyst and light source [35]. As a result, pure and metal doped catalysts have the capacity to degrade under irradiating light energy. The synthesized pure and doped TiO_2 catalysts for the degradation of methylene blue (MB) and methyl orange (MO) dyes with irradiation time of 60 min under UV light and its efficiency is calculated from Eq. (1) and the values are shown in Table 2. The degradation was attained for all the samples with an increasing irradiation time. The doped TiO_2 samples show an excellent degradation of MB and MO in the same UV light when compared with pure, since the dopant metal ions have an impact to generate more electrons and holes. These in turn promotes more degradation efficiency under UV light. The improved surface properties and the smaller crystallite size of the doped catalysts have the probable electron transfer properties which increases the photocatalytic activity [36–37]. On the other hand, the degradation of dyes depends on the shape factor of the synthesized particles [38–39]. It has been reported from the literatures that the spherical shape of the particle having large surface area plays a substantial role for organic dye degradation [40]. The literature report of Kaneva et al. had shown comparing with the crystallite size, the morphology of the prepared samples revealed

Table 2
Degradation efficiency of all prepared samples under UV and visible light irradiation.

Samples	Degradation efficiency of MO in 60 min under UV light (%)	Degradation efficiency of MB in 60 min under UV light (%)	Degradation efficiency of MO in 240 min under visible light (%)	Degradation efficiency of MB in 240 min under visible light (%)
Pure TiO_2	65.3	72.4	4.1	6.2
Mn doped TiO_2	85.2	93.6	65.2	73.2
Co doped TiO_2	78.2	86.4	53.2	64.3
Zr doped TiO_2	70.1	77.3	22.6	38.2

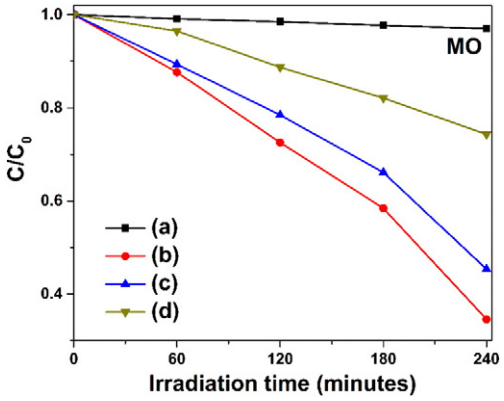

Fig. 8. Time course degradation of MO under visible light using a) pure TiO_2, b) Mn doped TiO_2, c) Co doped TiO_2 and d) Zr doped TiO_2.

greater influence on surface properties. [41]. Saravanan et al. had displayed the uniform spherical shaped nanoparticle morphology synthesized by chemical precipitation method which influences better photocatalytic activity with enhanced efficiency compared to the thermal decomposition method of synthesizing rod shaped nanoparticles. [42].

In our work, maximum efficiency is achieved for Mn doped TiO_2 sample for both MB and MO dyes than pure and metal doped TiO_2 because of its higher surface area [13–16,19]. In the case of MB degradation under UV light irradiation, Mn doped TiO_2 sample shows 21% more efficiency than pure TiO_2 sample. Similarly, followed by 7% higher efficiency than Co doped sample and 16% than Zr doped sample. For MO degradation, Mn doped TiO_2 sample provides 20% more efficiency than pure TiO_2 sample, 7% than Co doped sample and 15% than Zr doped TiO_2 sample. On evaluating the degradation of both the dyes, MB has resulted in higher efficiency than MO for both pure TiO_2 and metal doped TiO_2 samples. The simple structure of MB provides an efficient degradation of the samples in which it enhances the photocatalytic reactions [40]. Moreover, MB acts as a sensitizer and so it degrades quicker than MO [42].

The visible light irradiated time course degradation curves for MB and MO with 240 min irradiation time were given in the Figs. 7 and 8. The efficiency percentages for degradation of dyes are given in Table 2. For MB degradation, Mn doped sample has 8.9% higher than Co doped sample and 35% than Zr doped sample. Similar observation has obtained for MO degradation too. Mn doped sample exhibits an increase of 12% than Co doped sample and 42% than Zr doped sample. Pure TiO_2 sample exhibits very less degradation in visible light due to its large band gap properties. [43–44].

The photocatalytic first order rate constants (k) were deliberated from the following equation [36]:

$$k = \ln(C/C_0)/t \quad (4)$$

where C and C_0 are the irradiation and initial concentrations of MO/MB dyes. The first order rate constant values of the prepared catalysts were tabulated which was shown in SI 1. In both UV and visible light irradiation, the calculated first order rate constant (k) values were undoubtedly specified that the Mn doped TiO_2 has superior degradation rate when compared with Co and Zr doped TiO_2 as well as pure TiO_2 material.

Furthermore, recycling process of the superior photocatalyst Mn doped TiO_2 material is essential to describe the long term environmental usability and find the stability of the catalyst. The result of three times recycling process of MO using Mn doped TiO_2 material under visible light irradiation is shown in SI 2 and the results obviously described very small variation. Hence, it was specified that the Mn doped TiO_2 material shows good stability and long term reusability for photocatalytic degradation of dyes under visible light irradiation.

The visible light photocatalytic pathway mechanism is denoted in the schematic diagram as shown in Fig. 9.

For the period of visible light irradiation on the doped TiO_2 surface, the electrons in the intermediate states are excited since the dopant metal ions created intermediate states in the TiO_2 structure, thus have sufficient energy to access more visible light absorption and transfer electrons to TiO_2 surface that stimulate more electrons under visible light which in turn advances the redox reactions [13,15–21]. These properties of the doped metal ions improve the photocatalytic reactions. Concurrently, transfer of electrons takes place from the valence band to

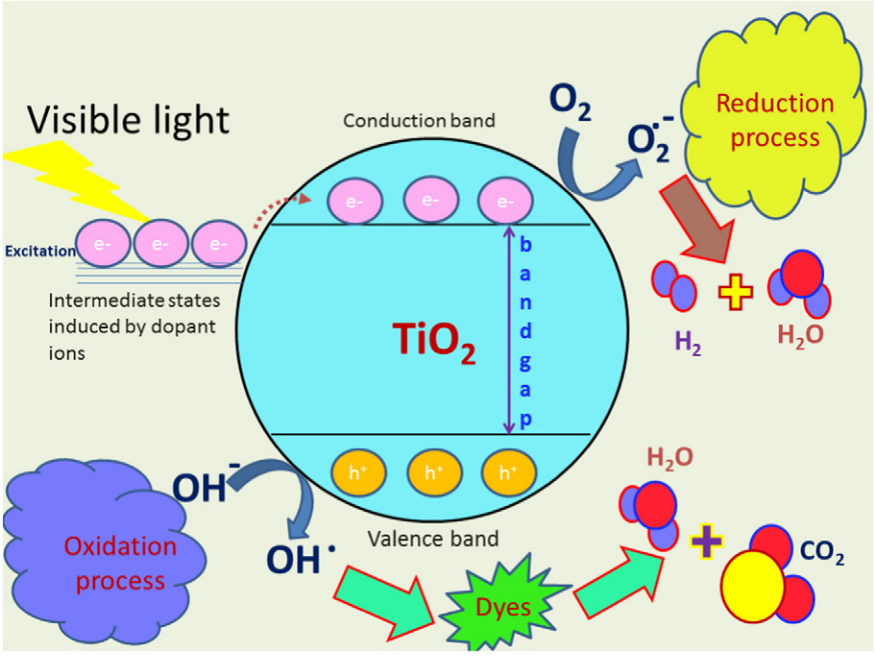

Fig. 9. The mechanism of visible light photocatalytic activity of doped TiO_2.

the conduction band by creating holes in the former and these holes in turn react with water molecules present in the dye and helps in the formation of OH radicals [15–21]. These OH radicals were supportive and significantly successful in degrading the dyes under visible light irradiation [45–64].

From the photocatalytic results, it is concluded that Mn doped sample shows extraordinary performance than the others and so it can be used for environmental applications. The major distinguishing parameters for the effective decomposition of organic species under light irradiation were the synthesis method, shape, the concentration of dopant materials, high surface area, the energy level and distribution of the dopant within TiO_2 structure [26,30,32,36].

4. Conclusion

This paper reports the effective synthesis of nanosized TiO_2 and (Mn, Co and Zr) doped TiO_2 by sol-gel method. The samples were characterized by different techniques and their degradation efficiencies were compared under the MB and MO dyes for both ultraviolet and visible light illuminance. The pure and doped TiO_2 exhibits the anatase phase tetragonal structure and showed agglomerated spherical shaped nanoparticles. The doped samples have wavelengths in the red region, while the pure sample has in the blue region of shorter wavelength. Because of the wide band gap 3.25 eV of pure TiO_2, it was unable to excite electrons to higher level during visible light photocatalytic reactions. Meanwhile, the doped samples have increased surface area with smaller crystallite size which favors the photocatalytic reactions. Thus the doped samples are likely to increase photocatalytic activity under visible light, since it has intermediate states in the TiO_2 lattice by preventing electron-hole pairs. Investigating among the doped TiO_2 under both ultraviolet and visible light irradiance, Mn doping promotes more degrading efficiency for both MB and MO while the Co and Zr doped samples have decreased activity. From overall study of the pure and doped TiO_2 samples; increased surface area, smaller crystallite size and reduced band gap of the doped samples have come up with the best photocatalytic efficiencies under visible light.

Acknowledgements

We acknowledge SAIF-IIT Chennai, India for FE-SEM characterization. The authors (R.S., F.G.) acknowledge the support of CONICYT through the project CONICYT/FONDECYT/3150631 and the postdoctoral fellowship granted to R.S.

Appendix A. Supplementary data

Supplementary data to this article can be found online at http://dx.doi.org/10.1016/j.molliq.2016.08.105.

References

[1] M. Grung, et al., Pesticide levels and environmental risk in aquatic environments in China - a review, Environ. Int. 81 (2015) 87–97.
[2] E. Neyens, J. Baeyens, A review of classic Fenton's peroxidation as an advanced oxidation technique, J. Hazard. Mater. 98 (2003) 33–50.
[3] J. Schneider, et al., Understanding TiO_2 photocatalysis: mechanisms and materials, Chem. Rev. 114 (19) (2014) 9919–9986.
[4] M. Ahmed, G. Xinxina, A review of metal oxynitrides for photocatalysis, Inorg. Chem. Front. 3 (2016) 578–590.
[5] V.K. Gupta, I. Ali, T.A. Saleh, A. Nayak, S. Agarwal, Chemical treatment technologies for waste-water recycling-an overview, RSC Adv. 2 (2012) 6380–6388.
[6] A. Fujishima, K. Honda, Electrochemical photolysis of water at a semiconductor electrode, Nature 238 (1972) 37–38.
[7] M.R. Hoffmann, S.T. Martin, W. Choi, D.W. Bahnemann, Environmental applications of semiconductor photocatalysis, Chem. Rev. 95 (1) (1995) 69–96.
[8] M. Pelaez, et al., A review on the visible light active titanium dioxide photocatalysts for environmental applications, Appl. Catal. B Environ. 125 (2012) 331–349.
[9] O. Ola, M.M. Maroto-Valer, Review of material design and reactor engineering on TiO_2 photocatalysis for CO_2 reduction, J Photochem Photobiol C: Photochem Rev 24 (2015) 16–42.
[10] T. Luttrell, et al., Why is anatase a better photocatalyst than rutile? - model studies on epitaxial TiO_2 films, Sci. Rep. 4 (4043) (2014) 1–8.
[11] C.G. Silva, J.L. Faria, Anatase vs. rutile efficiency on the photocatalytic degradation of clofibric acid under near UV to visible irradiation, Photochem. Photobiol. Sci. 8 (2009) 705–711.
[12] B. Liu, et al., Large-scale synthesis of transition-metal-doped TiO_2 nanowires with controllable overpotential, J. Am. Chem. Soc. 135 (27) (2013) 9995–9998.
[13] L.G. Devi, B.N. Murthy, S.G. Kumar, Photocatalytic activity of TiO_2 doped with Zn^{2+} and V^{5+} transition metal ions: influence of crystallite size and dopant electronic configuration on photocatalytic activity, Mater. Sci. Eng. B 166 (2010) 1–6.
[14] D.H. Kim, D.K. Choi, S.J. Kim, K.S. Lee, The effect of phase type on photocatalytic activity in transition metal doped TiO_2 nanoparticles, Catal. Commun. 9 (2008) 654–657.
[15] S.N.R. Inturi, T. Boningari, M. Suidan, P.G. Smirniotis, Visible-light-induced photodegradation of gas phase acetonitrile using aerosol-made transition metal (V, Cr, Fe, Co, Mn, Mo, Ni, Cu, Y, Ce, and Zr) doped TiO_2, Appl. Catal. B Environ. 144 (2014) 333–342.
[16] B. Gao, T.M. Lim, D.P. Subagio, T.T. Lim, Zr-doped TiO_2 for enhanced photocatalytic degradation of bisphenol A, Appl. Catal. A Gen. 375 (2010) 107–115.
[17] J. Choina, et al., Photocatalytic properties of Zr-doped titania in the degradation of the pharmaceutical ibuprofen, J. Photochem. Photobiol. A Chem. 274 (2014) 108–116.
[18] G. Sadanandam, K. Lalitha, V.D. Kumari, M.V. Shankar, M. Subrahmanyam, Cobalt doped TiO_2: a stable and efficient photocatalyst for continuous hydrogen production from glycerol: water mixtures under solar light irradiation, Int. J. Hydrog. Energy 38 (2013) 9655–9664.
[19] Q.R. Deng, X.H. Xia, M.L. Guo, Y. Gao, G. Shao, Mn-doped TiO_2 nanopowders with remarkable visible light photocatalytic activity, Mater. Lett. 65 (2011) 2051–2054.
[20] T.H. Kim, et al., Synthesis of solar light responsive Fe, N co-doped TiO_2photocatalyst by sonochemical method, Catal. Today 212 (2013) 75–80.
[21] G. Murtaza, et al., Structural and magnetic studies on Zr doped ZnO diluted magnetic semiconductor, Curr. Appl. Phys. 14 (2014) 176–181.
[22] W. Zhang, et al., Mn-doped TiO_2 nanosheet-based spheres as anode materials for lithium-ion batteries with high performance at elevated temperatures, ACS Appl. Mater. Interfaces 6 (10) (2014) 7292–7300.
[23] B. Choudhury, A. Choudhury, Luminescence characteristics of cobalt doped TiO_2 nanoparticles, J. Lumin. 132 (2012) 178–184.
[24] B. Choudhury, A. Choudhury, Oxygen vacancy and dopant concentration dependent magnetic properties of Mn doped TiO_2 nanoparticle, Curr. Appl. Phys. 13 (2013) 1025–1031.
[25] W. Alamgir, S. Khan, M. Ahmad, M. Hassan, A.H. Naqvi, Structural phase analysis, band gap tuning and fluorescence properties of Co doped TiO_2 nanoparticles, Opt. Mater. 38 (2014) 278–285.
[26] Y. Cong, J. Zhang, F. Chen, M. Anpo, D. He, Preparation, photocatalytic activity, and mechanism of nano-TiO_2 Co-doped with nitrogen and iron (III), J. Phys. Chem. C 111 (28) (2007) 10618–10623.
[27] S.W. Kim, R. Khan, T.J. Kim, W.J. Kim, Synthesis, characterization, and application of Zr, S Co-doped TiO_2 as visible-light active photocatalyst, Bull. Kor. Chem. Soc. 29 (6) (2008) 1217–1223.
[28] S. Mugundan et al. Synthesis and characterization of undoped and cobalt-doped TiO_2 nanoparticles via sol–gel technique, Appl. Nanosci. doi: http://dx.doi.org/10.1007/s13204-014-0337-y.
[29] H.Y. Wang, et al., High-surface-area mesoporous TiO_2 microspheres via one-step nanoparticle self-assembly for enhanced lithium-ion storage, Nanoscale 6 (2014) 14926–14931.
[30] R. Saravanan, N. Karthikeyan, V.K. Gupta, P. Thangadurai, V. Narayanan, A. Stephen, ZnO/Ag nanocomposite: an efficient catalyst for degradation studies of textile effluents under visible light, Mater. Sci. Eng. C 33 (2013) 2235–2244.
[31] S.A. Bakar, G. Byzynski, C. Ribeiro, Synergistic effect on the photocatalytic activity of N-doped TiO_2 nanorods synthesised by novel route with exposed (110) facet, J. Alloys Compd. 666 (2016) 38–49.
[32] R. Saravanan, V.K. Gupta, V. Narayanan, A. Stephen, Visible light degradation of textile effluent using novel catalyst ZnO/γ-Mn_2O_3, J. Taiwan Inst. Chem. Eng. 45 (2014) 1910–1917.
[33] S. Pan, et al., Engineering the intermediate band states in amorphous Ti^{3+}-doped TiO_2 for hybrid dye-sensitized solar cell applications, J. Mater. Chem. A 3 (2015) 11437–11443.
[34] M. Khairy, W. Zakaria, Effect of metal-doping of TiO_2 nanoparticles on their photocatalytic activities toward removal of organic dyes, Egypt. J. Pet. 23 (2014) 419–426.
[35] L. Gnanasekaran, R. Hemamalini, K. Ravichandran, Synthesis and characterization of TiO2 quantum dots for photocatalytic application, J. Saudi Chem. Soc. 19 (2015) 589–594.
[36] R. Saravanan, et al., ZnO/Ag/CdO nanocomposite for visible light-induced photocatalytic degradation of industrial textile effluents, J. Colloid Interface Sci. 452 (2015) 126–133.
[37] H. Wang, et al., Comparison of dye degradation efficiency using ZnO powders with various size scales, J. Hazard. Mater. 141 (2007) 645–652.
[38] J. Xie, Y. Li, W. Zhao, L. Bian, Y. Wei, Simple fabrication and photocatalytic activity of ZnO particles with different morphologies, Powder Technol. 207 (2011) 140–144.
[39] Y. Wang, X. Li, G. Lu, G. Chen, Y. Chen, Synthesis and photo-catalytic degradation property of nanostructured-ZnO with different morphology, Mater. Lett. 62 (2008) 2359–2362.
[40] R. Saravanan, V.K. Gupta, V. Narayanan, A. Stephen, Comparative study on photocatalytic activity of ZnO prepared by different methods, J. Mol. Liq. 181 (2013) 133–141.

[41] N. Kaneva, et al., Photocatalytic activity of nanostructured ZnO films prepared by two different methods for the photoinitiated decolorization of malachite green, J. Alloys Compd. 500 (2010) 252–258.
[42] R. Saravanan, H. Shankar, G. Rajasudha, V. Narayanan, A. Stephen, Photocatalytic degradation of organic dye using nano ZnO, Int. J. Nanosci. 10 (2011) 253–257.
[43] C. Yu, G. Li, S. Kumar, H. Kawasaki, R. Jin, Stable Au25(SR)18/TiO_2 composite nanostructure with enhanced visible light photocatalytic activity, J. Phys. Chem. Lett. 4 (2013) 2847–2852.
[44] H. Huang, et al., Efficient photocatalytic activity of PZT/TiO2 heterojunction under visible light irradiation, J. Phys. Chem. C 113 (2009) 14264–14269.
[45] R. Saravanan, et al., Conducting PANI stimulated ZnO system for visible light photocatalytic degradation of colour dyes, J. Mol. Liq. 221 (2016) 1029–1033.
[46] R. Saravanan, et al., Excellent visible light photocatalytic activity of β - $Ag_{0.333}V_2O_5$ nanorods by facile thermal decomposition method, J. Saudi Chem. Soc. 19 (2015) 521–527.
[47] R. Saravanan, et al., ZnO/CdO nanocomposites for textile effluent degradation and electrochemical detection, J. Mol. Liq. 209 (2015) 374–380.
[48] R. Saravanan, H. Shankar, T. Prakash, V. Narayanan, A. Stephen, ZnO/CdO composite nanorods for photocatalytic degradation of methylene blue under visible light, Mater. Chem. Phys. 125 (2011) 277–280.
[49] R. Saravanan, et al., Enhanced photocatalytic activity of ZnO/CuO nanocomposites for the degradation of textile dye on visible light illumination, Mater. Sci. Eng. C 33 (2013) 91–98.
[50] T.A. Saleh, V.K. Gupta, Column with CNT/Magnesium oxide composite for lead (II) removal from water, Environ. Sci. Pollut. Res. 19 (2012) 1224–1228.
[51] V.K. Gupta, S.K. Srivastava, D. Mohan, S. Sharma, Design parameters for fixed bed reactors of activated carbon developed from fertilizer waste material for the removal of some heavy metal ions, Waste Manag. 17 (1998) 517–522.
[52] V.K. Gupta, A. Mittal, J. Mittal, Decoloration treatment of a hazardous triaryl methane dye, light green sf (yellowish) by waste material adsorbents, J. Colloid Interface Sci. 342 (2010) 518–527.
[53] V.K. Gupta, A. Mittal, D.K.A. Malviya, J. Mittal, Adsorption studies on the removal of colouring agent phenol red from wastewater using waste materials as adsorbents, J. Colloid Interface Sci. 337 (2009) 345–354.
[54] A. Mittal, A. Malviya, J. Mittal, V.K. Gupta, Adsorptive removal of hazardous anionic dye 'congo red' from wastewater using waste materials and recovery by desorption, J. Colloid Interface Sci. 340 (2009) 16–26.
[55] V.K. Gupta, S. Agarwal, T.A. Saleh, Synthesis and characterization of alumina-coated carbon nanotubes and their application for lead removal, J. Hazardous Mat. 185 (2011) 17–23.
[56] V.K. Gupta, I. Ali, T.A. Saleh, A. Nayak, S. Agarwal, Chemical treatment technologies for wastewater recycling –a review, RSC Adv. 2 (2012) 6380–6388.
[57] V.K. Gupta, A. Mittal, J. Mittal, Removal and recovery of chrysoidine y from aqueous solutions by waste materials, J. Colloid Interface Sci. 344 (2010) 497–507.
[58] V.K. Gupta, R. Jain, Shilpi Agarwal, M. Shrivastava, Removal of the hazardous dye - tartrazine by photodegradation on titanium dioxide surface, Mater. Sci. Eng. C 31 (2011) 1062–1067.
[59] V.K. Gupta, A. Nayak, Cadmium removal and recovery from aqueous solutions by novel adsorbents prepared from orange peel and Fe_2O_3 nanoparticles, Chem. Eng. J. 180 (2012) 81–90.
[60] T.A. Saleh, V.K. Gupta, Photo-catalyzed degradation of hazardous dye methyl orange by use of a composite catalyst consisting of multiwalled carbon nanotubes and titanium dioxide, J. Colloids Interface Sci. 371 (2012) 101–106.
[61] H. Khani, M.K. Rofouei, P. Arab, V.K. Gupta, Z. Vafaei, Multi-walled carbon nanotubes-ionic liquid-carbon paste electrode as a super selectivity sensor: Application to potentiometric monitoring of mercury ion (II), J. Hazard. Mater. 183 (2010) 402–409.
[62] V.K. Gupta, A. Mittal, D. Jhare, J. Mittal, Batch and bulk removal of hazardous colouring agent rose bengal by bottom ash, RSC Adv. 2 (2012) 8381–8389.
[63] V.K. Gupta, T.A. Saleh, Functionalization of tungsten oxide into MWCNT and its application as a novel catalyst for sun-light-induced degradation of rhodamine B, J. Colloids Interface Sci. 362 (2011) 337–344.
[64] V.K. Gupta, T.A. Saleh, Environmental science and pollution research, 20 (5) (2013) 2828–2843.